Photo-double-ionization of the nitrogen molecule

P. Bolognesi,[1] B. Joulakian,[2] A. A. Bulychev,[3] O. Chuluunbaatar,[3,4] and L. Avaldi[1]

[1]*CNR- Istituto di Metodologie Inorganiche e dei Plasmi, Area della Ricerca di Roma 1, CP 10, 00015 Monterotondo Scalo, Italy*

[2]*Université de Lorraine, SRSMC (UMR CNRS 7565), 1 boulevard Arago, bâtiment ICPM, 57078 Metz Cedex 3, France*

[3]*Joint Institute for Nuclear Research, Dubna, Moscow Region 141980, Russia*

[4]*National University of Mongolia, Ulaanbaatar, Mongolia*

(Received 24 January 2014; published 7 May 2014)

The triple differential cross sections of the photo-double-ionization of the nitrogen molecule to the $X\ ^1\Sigma^+_g$ and $a^3\Pi_u$ N_2^{2+} states have been measured at about 20 eV above their respective ionization thresholds in the equal energy sharing kinematics and calculated using a model which makes use of correlated two-center double continuum wave functions. The comparison of the results with those obtained by the Gaussian parametrization method applied in the past with success to heliumlike targets shows the influence of the molecular nature of the N_2 target in the photo-double-ionization.

DOI: 10.1103/PhysRevA.89.053405 PACS number(s): 33.80.Eh, 33.20.−t

I. INTRODUCTION

The study of the emission of two electrons from an isolated system by absorption of a single energetic photon, i.e., the photo-double-ionization (PDI) process, has attracted a lot of interest mainly because it represents a unique experimental mean to probe electron-electron interaction in atoms and molecules. These experiments, during which either the two photoelectrons, after angle and energy selection, or one of the photoelectrons and the recoiling ion are detected in coincidence, provide the most detailed information on the electronic structure and the mechanisms of ionization via the measurement of the triple differential cross section (TDCS), which is directly related to the probability of the events. The study of the PDI of helium, the simplest two-electron system, challenged for a long time both experimentalists and theorists and showed that the dynamics of the electron pair is strongly constrained by its own symmetry and the Coulomb repulsion [1–3].

The PDI of molecules is significantly more complex and introduces new physical effects. In the simplest two-electron molecule, H_2, for example, there is no unique double-ionization threshold, which depends on the internuclear separation as the upper repulsive potential curve is purely Coulombic, while the ground state electronic configuration is inevitably more complex as a result of the two-center nuclear potential. Here the PDI is followed by a "Coulomb explosion" as the two protons rapidly dissociate. In such a case, energy- and angle-resolved detection of all four particles [4–7], with a well-defined light polarization state, is needed to define completely the PDI dynamics. While fully differential cross sections for aligned molecules [4–7] or TDCS for randomly oriented molecules [8–11] have been determined in the cases of H_2 and D_2, no attempts have been reported for the determination of the TDCS of the PDI of other more complex molecules. Some efforts, based on electron-electron [12,13] and ion-ion coincidence experiments [14] have been devoted to the determination of the electronic structure of dications. In this paper, we report the results of an investigation of the TDCS of randomly oriented N_2 molecules. The diatomic nitrogen molecule has been chosen because the lowest states are metastable as proven by the vibrational progressions observed by Dawber *et al.* [12], Eland [13], and Ahmad *et al.* [15]. Moreover, Bulychev *et al.* [16] have recently extended a theoretical approach that makes use of the two-center double continuum wave function developed for the $(e,3e)$ double ionization [17] to the case of the photo-double-ionization.

II. EXPERIMENT

The experiments reported in this paper have been performed using the electron-electron multicoincidence end-station [18] at the gas phase photoemission [19] beamline of the Elettra storage ring, where an undulator of period 12.5 cm and 4.5 m long produces completely linearly polarized radiation in the photon energy range 13–1000 eV with a typical resolving power of 10 000. In the present case the energy resolution was degraded to about 150 meV in order to increase the photon flux, that in these conditions was measured to be of the order of 4×10^{12} photon/s. The vacuum chamber hosts two independent turntables, holding respectively three and seven electrostatic hemispherical analyzers spaced by 30°. The three spectrometers of the smaller turntable are mounted at angles of 0°, 30°, and 60° with respect to the polarization vector of the light $\boldsymbol{\varepsilon} = \varepsilon \boldsymbol{x}$ and they have been used to measure "the "fixed electron," labeled 1, in the perpendicular plane. The larger turntable rotates in the plane perpendicular to the direction, **z**, of propagation of the incident radiation, and its seven analyzers have been used to measure the angular distribution of the correlated electron, labeled 2, of complementary energy in order to fulfill the energy balance $E_1 + E_2 = h\nu - I^{2+}$, where I^{2+} is the double-ionization potential. The ten analyzers have been set to detect electrons of kinetic energy $E_1 = E_2 =$ 10.5 eV. The energy resolution and the angular acceptance in the dispersion plane of the spectrometers were $\Delta E/E_{1,2} =$ 0.03 and $\Delta\theta_{1,2} = \pm 3^\circ$, respectively. Therefore the overall energy resolution was about 450 meV in the measurement of the energy spectrum and about 310 meV in the measurements of the angular distributions.

Two types of measurements have been performed. In the first one, the photon energy has been scanned and the energy spectrum of the N_2 dication states is reconstructed. In order to improve the statistical accuracy of the experimental results, the coincidence signals of the 21 photoelectron-photoelectron pairs were added up, after a careful energy calibration of the

noncoincidence spectra independently collected by the ten analyzers. Then at fixed values of the photon energy the TDCS have been measured. The relative angular efficiency of the ten analyzers has been established and checked by measuring the photoelectron angular distributions for photoionization of Ne $2p$ and He $1s$ electrons, with well-known asymmetry parameters, at the same excess energy above their respective ionization thresholds [20,21]. The same efficiency correction has been assumed for the coincidence measurements. The validity of this assumption was tested by measuring the coincidence yield at two positions of the larger turntable that overlap two nearby analyzers and confirmed by comparing the coincidence yield measured by different pairs of analyzers in complementary kinematics [18]. Therefore, all the experimental data are cross-normalized and can be reported on the same relative scale of counts.

At the typical experimental conditions of about 10^{13} mol/cm^3 the typical true coincidence count rate was 1−3 mHz and acquisition times of about 3.5 h/point were needed in order to achieve the present accuracy in the measurements of the TDCS.

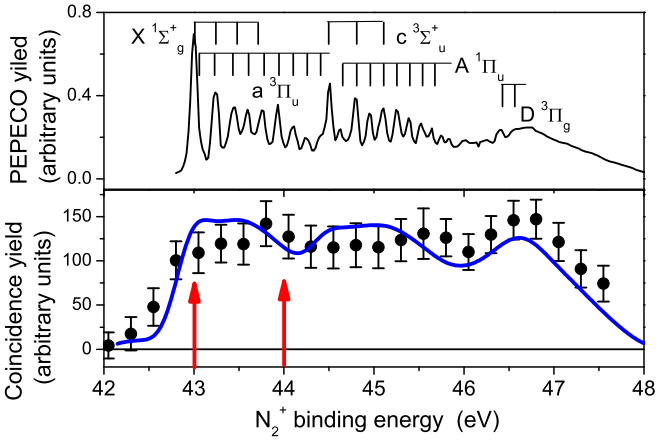

FIG. 1. (Color online) Binding energy spectrum of N_2 dication measured in the present experiment (dots with error bars, bottom panel) and in the PEPECO experiment of Ref. [13] (top panel). The solid line in the bottom panel is the convolution of the PEPECO [13] experiment with a Gaussian function FWHM = 400 meV. The two arrows indicate the values of binding energy where the TDCS have been measured.

III. THEORY

The theory for the PDI of diatomic molecules has been recently presented elsewhere [16]. Here only some details relevant to the present work are reported. The fully differential cross section, FDCS, for the detection of the two ejected electrons from a diatomic molecule is given by

$$\mathrm{FDCS}(\rho) = \frac{d\sigma}{d\Omega_\rho d\Omega_1 d\Omega_2 d\left(\frac{k_1^2}{2}\right)} = \frac{4\pi^2}{\omega}\alpha k_1 k_2 |T_{\mathrm{fi}}|^2, \quad (1)$$

where $d\Omega_1$ and $d\Omega_2$, are, respectively, the elements of the solid angles for the orientations of the ejected electrons; ρ represents the direction of the internuclear axis; k_1 and k_2 represent the moduli of the wave vectors of the ejected electrons; $\alpha = 1/137.035\,99$ is the fine-structure constant; and ω is the photon frequency. In the case of randomly oriented targets, the FDCS has to be integrated over all possible and equally probable orientations of the molecule in space to produce the measured TDCS:

$$\mathrm{TDCS} = \frac{1}{4\pi}\int d\Omega_\rho \mathrm{FDCS}(\rho). \quad (2)$$

In the transition matrix element T_{fi} a correlated product of two-center continuum (TCC) wave function [22], describing the double continuum of the two ejected photoelectrons in the field of the two Coulomb centers, was used [17]. For the initial electronic state wave function of the nitrogen molecule, Hartree-Fock diatomic orbitals were employed, which were obtained [16] by the construction of linear combinations of atomic orbitals [23–25].

IV. RESULTS AND DISCUSSION

In the bottom panel of Fig. 1 the binding energy spectrum measured in the present experiment is shown. On the top panel of the same figure, the spectrum measured in the photoelectron-photoelectron-coincidence (PEPECO) experiment by Eland [13] at 48 eV photon energy, as digitized from Fig. 2 of that work, is reported. This spectrum is characterized by a series of peaks, which can be assigned to the vibrational series of a few electronic states according to the calculated potential energy curves [14]. The first peak at about 43 eV is assigned to the $X\ ^1\Sigma^+_g$ ground state. Its short vibrational progression, characterized by a quantum of about 250 meV, is strongly overlapping with the long vibrational progression of the first excited $a^3\Pi_u$, state, whose spacing is about 180 meV. These are the two relevant states for the present work. The high resolution PEPECO spectrum [13] has been convoluted with a Gaussian function of 400 meV full width at half maximum (FWHM) to simulate the energy resolution of our experiment and compared with the present spectrum in the bottom panel of Fig. 1. Despite the fact that the different excitation energies might result in different populations of the N_2^{2+} states, a reasonable agreement between the two spectra is observed.

The TDCS have been measured at binding energies of about 43 and 44 eV, as shown by the vertical arrows in Fig. 1. Considering the energy resolution, in the first experiment we have sampled the $X\ ^1\Sigma^+_g$ ground state $v = 0$, with some contribution from the $v = 0$ and 1 of the $a^3\Pi_u$ state, while in second one the first excited $a^3\Pi_u$ state is studied.

The TDCS of the $X\ ^1\Sigma^+_g$ and $a^3\Pi_u$ states are shown in Figs. 2 and 3, respectively, where the theoretical predictions are also reported. In the insets of Figs. 2 and 3 the polar plots of the TDCS are reported too. In order to compare the shape of the measured and calculated TDCS the experiments have been normalized to the theory at $\theta_1 = 0°$ for both the states. The numbers in Figs. 2(b), 2(c), 3(b), and 3(c) are the multiplicative factors used to match the relative experimental TDCS and the calculated ones at $\theta_1 = 30°$ and 60°.

There is a reasonable agreement between theory and experiments as far as the shape of the TDCS is concerned, even though some discrepancies are observed. For $\theta_1 = 0°$ and $\theta_2 \sim 180°$ the experimental intensity is larger than the

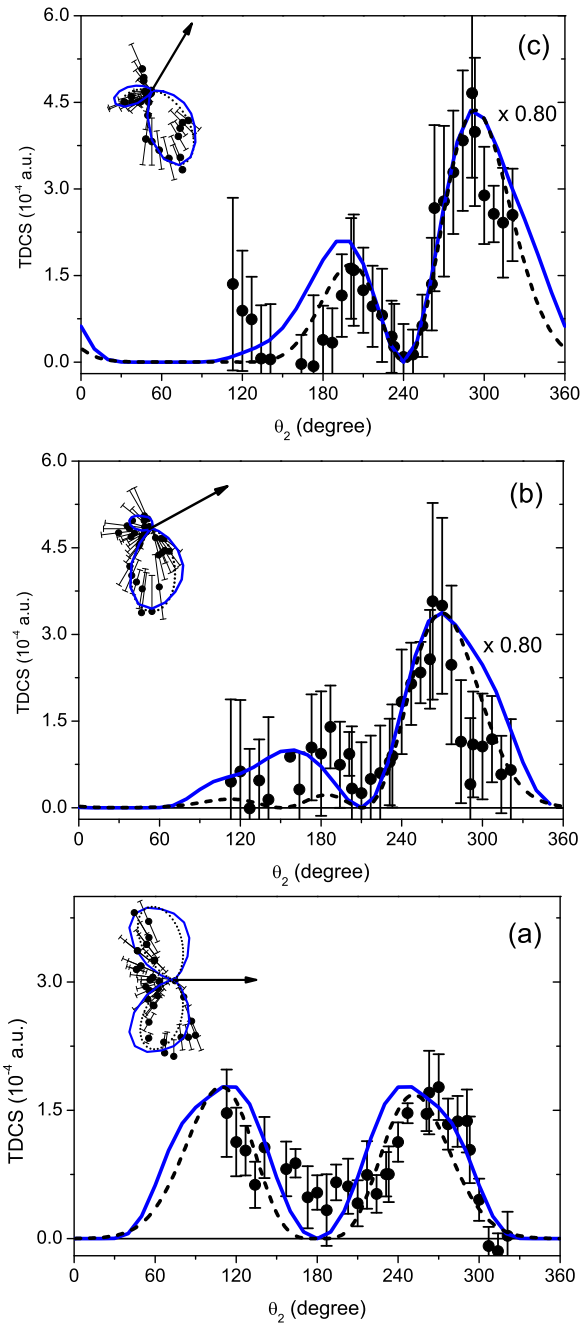

FIG. 2. (Color online) TDCS of the PDI of the $X\ ^1\Sigma^+_g$ state of N_2^{2+} in atomic units (a.u.) with $\theta_1 = 0$ (a), 30 (b), and 60° (c). The solid (blue) and dotted (black) lines represent the theoretical predictions of the model with two-center wave functions and those obtained by the Gaussian parametrization model, respectively. In the insets the polar representations of the TDCS are shown. The arrows indicate the direction θ_1 of the fixed electron. The numbers are the multiplicative factors used to match the relative experimental TDCS and the calculated ones.

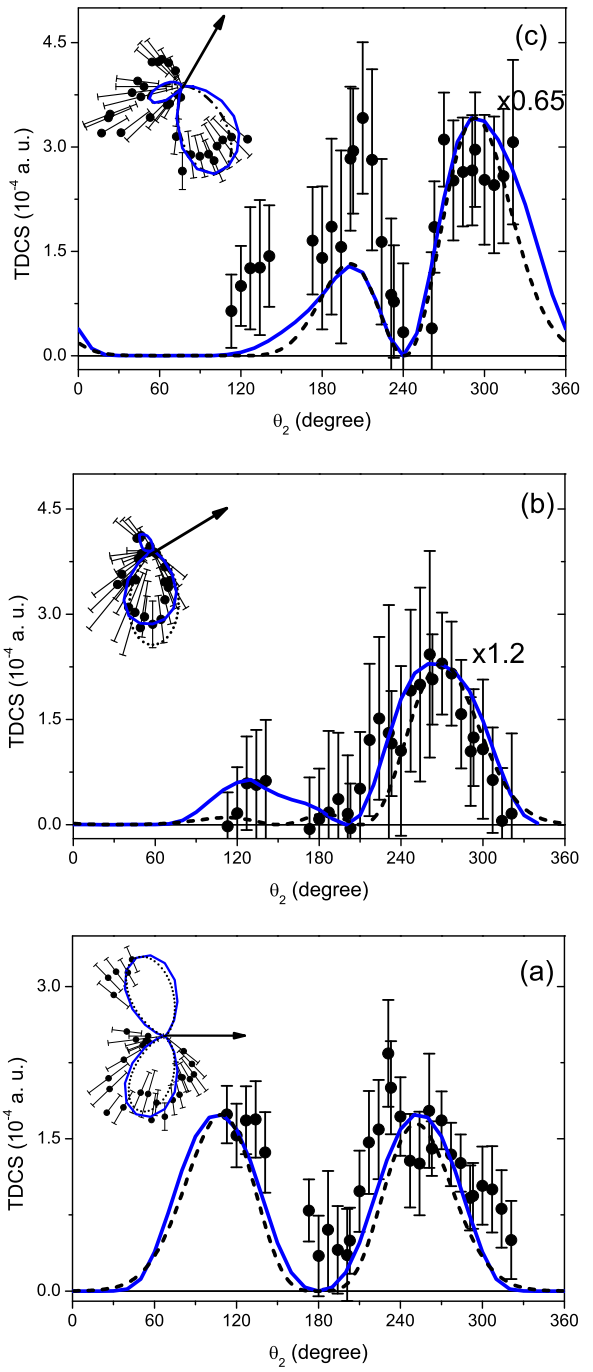

FIG. 3. (Color online) Same as Fig. 2 but for the $a^3\Pi_u$ state of N_2^{2+}.

calculated one for both states [see Figs. 2(a) and 3(a)]. At $\theta_1 = 0°$, theory predicts a smaller angle between the two lobes than in the experiment and a shoulder at a relative angle about 25° larger for the $^1\Sigma^+_g$ state not observed in the experiment, while the broadening of the lobe in the case of the $a^3\Pi_u$ state finds a good match in the experimental results. For the same state, at $\theta_1 = 60°$, Fig. 3(c), theory underestimates the lobe at $\theta_2 = 220°$. In all cases theory tends to overestimate the intensity going from $\theta_1 = 0°$ to 60° for the ground state, as shown by the multiplicative factors reported in Figs. 2 and 3, apart from the TDCS at $\theta_1 = 30°$ of the $a^3\Pi_u$ state where theory underestimates the experiment.

For the sake of comparison, the TDCS predicted by the parametrization model developed in the past [26] for the PDI of He for the same experimental conditions of the N_2 experiment are shown in Figs. 2 and 3. In the equal energy

sharing kinematic the He TDCS can be written as

$$\mathrm{TDCS}(E_1,E_2,\theta_{12}) \propto |a_g(E_1,E_2,\theta_{12})(\cos\theta_1+\cos\theta_2)|^2, \quad (3)$$

where θ_{12} is the relative angle between the two photoelectrons [1]. The θ_{12} and E dependence of the complex amplitude a_g includes all the physical information on the dynamics of the process, i.e., the effects of the electron-electron and electron-residual ion interactions. Based on Wannier-type theories [27], the symmetric amplitude a_g is usually represented by a Gaussian function,

$$|a_g| = A\exp[-2\ln 2(\theta_{12}-180)^2/\gamma^2] \equiv AG(\theta_{12},\gamma), \quad (4)$$

where γ is the correlation width. The Gaussian ansatz has been found to be a useful and valid approximation in the case of He up to an excess energy of 80 eV [28]. At an excess energy of about 20 eV, $\gamma = 90°$ [1].

The He TDCS have been rescaled independently to the maximum of each TDCS in Figs. 2(a)–2(c) and 3(a)–3(c). The shape of the He TDCS is quite consistent with the N_2 experimental ones, apart from the region close to $\theta_{12} = 180°$ and in the case of the minor lobe at $\theta_1 = 30°$. The calculations with the two-center continuum wave functions predict broader lobes than in He for the ground state of the dication, and for both states a more intense secondary lobe at $\theta_1 = 30°$. The general resemblance of the measured and calculated TDCS with respect to the atomic ones can be ascribed to the kinematics used. Indeed, the de Broglie wavelength associated with a 10.5 eV electron is about 7 a.u., definitely larger than the equilibrium internuclear distance of the N_2 molecule, which is about 2 a.u. Under such a condition the photoelectrons see the molecule as an atom.

The main difference between the N_2 experiments as well as the two-center calculations and the atomic TDCS is in the region close to $\theta_{12} = 180°$, where parity and exchange symmetry in the case of the He atom make the TDCS vanish. Reddish and Feagin [29] developed a basic description of the TDCS for diatomic molecules and derived a heliumlike expression that depends on the orientation of the internuclear axis at the time of the PDI, i.e., on the amplitudes for the excitation parallel and perpendicular to the molecular axis, $a_{\Sigma/\Pi}$. When applied to randomly oriented molecules the expression of the TDCS of this model is composed by two terms: one has the same form as that of the He TDCS, while the other term has the form $\frac{16}{15}\pi|a_\Sigma - a_\Pi|^2\cos^2(\theta_{12}/2)$ and is independent from the photon polarization direction. This molecular term produces a relaxation of the selection rules for atomic PDI [30]. The same authors [29] showed that, under the hypothesis that the molecular amplitudes can be represented by Gaussian functions, a study of the ratio TDCS(D_2)/TDCS(He) provides valuable information on the molecular term in the TDCS and on the ratio $\eta = a_\Pi/a_\Sigma$. In Fig. 4 the ratio with the He TDCS calculated with Eqs. (3) and (4) is shown for both N_2 dication states. The two ratios display the same trend, apart from the region $\theta_{12} < 60°$ where the one for the $a^3\Pi_u$ state seems to rise, while the other remains constant within the experimental uncertainty.

As shown in Ref. [29] the ratio in the case of the $X\,^1\Sigma^+_g$ state can be fitted by the expression $\frac{G_{N_2}(\theta_{12},\gamma_{N_2})}{G_{He}(\theta_{12},\gamma_{He})}[1+\frac{C(\eta)\tilde{T}_2(\theta_1,\theta_2)}{\tilde{T}_1(\theta_1,\theta_2)}]$, where the $\tilde{T}_i(\theta_1,\theta_2)$ ($i = 1$ and 2) functions are the geometrical parts of the molecular and atomic TDCS integrated over the θ_1 and θ_2 angular acceptancies [29] and $C(\eta) = \frac{4|1-\eta|^2}{2+7|\eta|^2+6\mathrm{Re}(\eta)}$. The free parameters for the fit were γ_{N_2} and the function $C(\eta)$, while the angular acceptance in θ_{12} was fixed to $\pm 7°$ and following Ref. [29] the two amplitudes were assumed to be real. The best fit, represented by the solid line in Fig. 4, gives $\gamma_{N_2} = 105° \pm 4°$ and $C(\eta) = 5.00 \pm 0.45$,

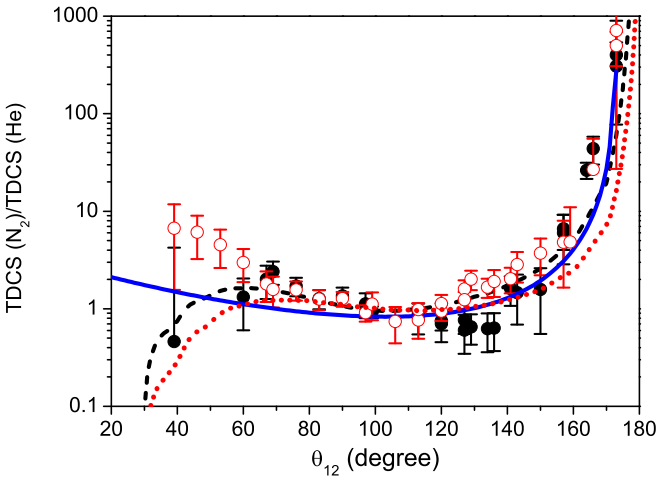

FIG. 4. (Color online) Ratio between the TDCS measured in N_2 (black dots, $X\,^1\Sigma^+_g$ state; red open circles, $a^3\Pi_u$ state) and the one calculated for He (Eqs. (3) and (4) with $\gamma = 90°$). The solid blue line is the fit to the experimental ratio of the $X\,^1\Sigma^+_g$ state using Eqs. (25) and (26) of Ref [29]. while the dash and dotted lines are the ratio using the N_2 TDCS for the $X\,^1\Sigma^+_g$ and $a^3\Pi_u$ states, respectively, calculated with the two-center wave-function model.

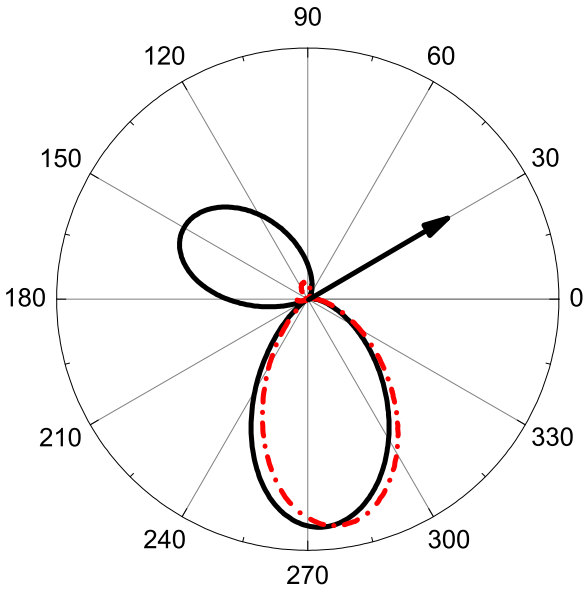

FIG. 5. (Color online) The TDCS of the $X\,^1\Sigma^+_g$ state of the $N_2{}^{2+}$ state at $\theta_1 = 30°$ calculated within the frame of the He-like model for diatomic molecules [29] with (black solid line) and without (red dash-dotted line) the molecular term. The values of $\gamma_{N_2} = 105°$ and $\eta = -0.19$ have been used.

which correspond to $\eta = -1.04 \pm 0.05$ and -0.19 ± 0.05, because η as a function of C is double valued. The negative value of η indicates that the a_Π and a_Σ amplitudes have a phase shift of 180°. η can be related to the ion angular asymmetry parameter $\beta_N = 2(1 - |\eta|^2)/(1 + |\eta|^2)$. The value $\eta = -1.04 \pm 0.05$ implies $\beta_N = -0.07 \pm 0.1$, i.e., an almost isotropic angular distribution, while the value $\eta = -0.19 \pm 0.05$ corresponds to $\beta_N = 1.86 \pm 0.08$, which indicates an angular distribution peaked along the polarization direction of the incident radiation.

In atoms, it is well established [31,32] that broader orbitals correspond to narrower correlation amplitudes. In the present case where the size of the orbitals of the nitrogen molecule is definitely broader than the He^+ one our fit leads to a broader correlation function than in He. This observation deserves further investigations either at different photon energies or in other molecular targets.

In Fig. 4 also the ratios (solid and dotted lines) determined using the TDCS calculated with two-center continuum wave function for both dication states are reported. The comparison with the experimental ratios clearly shows that this calculation takes into account a large fraction of the "molecular effect," although some differences are still observed for $\theta_{12} > 160°$. A departure from the experimental results is also observed in the region of small mutual angles, $\theta_{12} < 60°$, where the Coulomb repulsion dominates the interaction between the two escaping electrons.

The most important evidence of the relevance of the molecular term is given by its effect on the TDCS at $\theta_1 = 30°$, where the atomiclike model largely underestimates the minor lobe [Figs. 2(b) and 3(b)]. In Fig. 5 the TDCS calculated using the parameters obtained by the fit reported in Fig. 4 with and without the molecular term are compared. In the figure one sees that the effect of the molecular term is to change dramatically the relative intensity of the lobes, due to the breakdown of the selection rules [30].

V. CONCLUSIONS

In summary the TDCS of the metastable dication states of molecular nitrogen have been measured in equal energy sharing conditions. The measured TDCS for two states of different symmetry display main features similar to the ones of the atomic case. The observed differences are consistent with previous observations of TDCS for randomly oriented D_2 molecules and can be interpreted on the base of the helium-like TDCS model for diatomic molecules [29]. A calculation with a two-center wave function describes the main feature of the measured TDCS, but still misses a complete match with the experiments.

ACKNOWLEDGMENT

L.A. thanks A. S. Kheifets for useful discussions.

[1] L. Avaldi and A. Huetz, J. Phys. B: At. Mol. Opt. Phys. **38**, S861 (2005).
[2] J. S. Briggs and V. Schmidt, J. Phys. B: At. Mol. Opt. Phys. **33**, R1 (2000).
[3] L. Malegat, Phys. Scr., T **110**, 83 (2004).
[4] T. Weber *et al.*, Nature (London) **431**, 437 (2004).
[5] T. Weber *et al.*, Phys. Rev. Lett. **92**, 163001 (2004).
[6] M. Gisselbrecht, M. Lavollée, A. Huetz, P. Bolognesi, L. Avaldi, D. P. Seccombe, and T. J. Reddish, Phys. Rev. Lett. **96**, 153002 (2006).
[7] T. J. Reddish, J. Colgan, P. Bolognesi, L. Avaldi, M. Gisselbrecht, M Lavollée, M. S. Pindzola, and A. Heutz, Phys. Rev. Lett. **100**, 193001 (2008).
[8] T. J. Reddish, J. P. Wightman, M. A. MacDonald, and S. Cvejanovic, Phys. Rev. Lett. **79**, 2438 (1997).
[9] N. Scherer, H. Lorch, and V. Schmidt, J. Phys. B: At. Mol. Opt. Phys. **31**, L817 (1998).
[10] J. P. Wightman, S. Cvejanovic, and T. Reddish, J. Phys. B: At. Mol. Opt. Phys. **31**, 1753 (1998).
[11] D. P. Seccombe *et al.*, J. Phys. B: At. Mol. Opt. Phys. **35**, 3767 (2002).
[12] G. Dawber *et al.*, J. Phys. B: At. Mol. Opt. Phys. **27**, 2191 (1994).
[13] J. H. D. Eland, Chem. Phys. **294**, 171 (2003).
[14] M. Lundqvist, D. Edvardsson, P. Baltzer, and B. Wannberg, J. Phys. B: At. Mol. Opt. Phys. **29**, 1489 (1996).
[15] M. Ahmad *et al.*, J. Phys. B: At. Mol. Opt. Phys. **39**, 3599 (2006).
[16] A. A. Bulychev, O. Chuluunbaatar, A. A. Gusev, and B. Joulakian, J. Phys. B: At. Mol. Opt. Phys. **46**, 185203 (2013).
[17] O. Chuluunbaatar, A. A. Gusev, and B. Joulakian, J. Phys. B: At. Mol. Opt. Phys. **45**, 015205 (2012).
[18] P. Bolognesi *et al.*, J. Electron Spectrosc. Relat. Phenom. **141**, 105 (2004).
[19] R. R. Blyth *et al.*, J. Electron Spectrosc. Relat. Phenom. **101–103**, 959 (1999).
[20] S. H. Soutworth, A. C. Parr, J. E. Hardis, J. L. Dehmer, and D. M. P. Holland, Nucl. Instrum. Methods Phys. Res., Sect. A **246**, 782 (1986).
[21] B. Kämmerling, A. Hausmann, J. Laüger, and V. Schmidt, J. Phys. B: At. Mol. Opt. Phys. **25**, 4773 (1992).
[22] O. Chuluunbaatar *et al.*, J. Phys. B: At. Mol. Phys. **41**, 015204 (2008).
[23] R. K. Nesbet, J. Chem. Phys. **40**, 3619 (1964).
[24] P. E. Cade, K. D. Sales, and A. C. Wahl, J. Chem. Phys. **44**, 1973 (1966).
[25] C. W. Scherr, J. Chem. Phys. **23**, 569 (1955).
[26] A. Huetz, P. Selles, D. Waymel, and J. Mazeau, J. Phys. B: At. Mol. Phys. **24**, 1917 (1991).
[27] J. M. Feagin, J. Phys. B: At. Mol. Phys. **17**, 2433 (1984).
[28] A. S. Kheifets and I. Bray, Phys. Rev. A **65**, 022708 (2002).
[29] T. J. Reddish and J. M. Feagin, J. Phys. B: At. Mol. Opt. Phys. **32**, 2473 (1999).
[30] F. Maulbetsch and J. S. Briggs, J. Phys. B: At. Mol. Opt. Phys. **28**, 551 (1995).
[31] A. S. Kheifets, I. Bray, J. Colgan, and M. S. Pindzola, J. Phys. B: At. Mol. Opt. Phys. **44**, 011002 (2011).
[32] E. Sokell, P. Bolognesi, A. Kheifets, I. Bray, S. Safgren, and L. Avaldi, Phys. Rev. Lett. **110**, 083001 (2013).